Title: Deficiency of Orexin Receptor Type 1 in Dopaminergic Neurons Increases Novelty-Induced Locomotion and Exploration

Xing Xiao[1], Gagik Yeghiazaryan[2,3], Anna L. Cremer[4], Heiko Backes[4], Peter Kloppenburg[2,3], and A. Christine Hausen[1*]

1 Max Planck Institute for Metabolism Research, Department of Neuronal Control of Metabolism, Gleueler Strasse 50, 50931 Cologne, Germany

2 Excellence Cluster on Cellular Stress Responses in Aging Associated Diseases (CECAD) and Center for Molecular Medicine Cologne (CMMC), University of Cologne, Joseph-Stelzmann-Strasse 26, 50931 Cologne, Germany

3 Department of Biology, Institute for Zoology, University of Cologne, Zülpicher Strasse 47b, 50674 Cologne, Germany

4 Max Planck Institute for Metabolism Research, Multimodal Imaging of Brain Metabolism Group, Gleueler Strasse 50, 50931 Cologne, Germany

* Correspondence: Christine.hausen@sf.mpg.de

Abstract

Orexin signaling in the ventral tegmental area and substantia nigra promotes locomotion and reward processing, but it is not clear whether dopaminergic cells directly mediate these effects. We show that dopaminergic neurons in these areas mainly express orexin receptor subtype 1 (Ox1R). In contrast, only a minor population in the medial ventral tegmental area express orexin receptor subtype 2 (Ox2R). To analyze the functional role of Ox1R signaling in dopaminergic neurons, we deleted Ox1R specifically in dopamine transporter-expressing neurons of mice and investigated the functional consequences. The deletion of Ox1R increased locomotor activity and exploration during exposure to novel environments or when intracerebroventricularely injected with orexin. Spontaneous activity in home cages, anxiety, reward processing, and energy metabolism did not change. Positron emission tomography imaging revealed that Ox1R signaling in dopaminergic neurons affected distinct neural circuits depending on the stimulation mode. In line with an increase of neural activity in lateral paragigantocellular nucleus (LPGi) of $Ox1R^{\Delta DAT}$ mice, we found that dopaminergic projections innervate the LPGi in regions where the inhibitory dopamine receptor subtype D2 but not the excitatory D1 subtype resides. These data suggest a crucial regulatory role of Ox1R signaling in dopaminergic neurons in novelty-induced locomotion and exploration.

Key words: orexin, Ox1R, Ox2R, dopamine, locomotion, exploration, arousal

Introduction

Orexin neurons are exclusively located in the lateral hypothalamus (LH) and adjacent regions in the brain, including perifornical area, and dorsomedial and posterior hypothalamus (Soya & Sakurai, 2020). Abundant orexin fibers innervate the ventral tegmental area (VTA) and substantia nigra (SN), which together contain the majority of dopaminergic neurons in humans and rodents (Fadel & Deutch, 2002; Hrabovszky et al., 2013; Peyron et al., 1998). There are also some dopaminergic neurons in other brain regions, although not all of these neurons express the dopamine transporter (DAT) (Koblinger et al., 2018; Sharples et al., 2014; Turiault et al., 2007). Both the orexin and dopaminergic systems control food intake, locomotor activity, reward processing as well as energy metabolism (Howe & Dombeck, 2016; Inutsuka & Yamanaka, 2013; Narayanan et al., 2010; Palmiter, 2007; Tsujino & Sakurai, 2013). The nigrostriatal dopaminergic system, containing the dopaminergic projections from SN to the dorsal striatum, predominantly regulates action selection and exploratory behaviors, while the mesolimbic and mesocortical dopaminergic systems, which consist of the dopaminergic pathways from the VTA to ventral striatum and prefrontal cortex, predominantly regulate motivation, cognition, reward, and aversion signaling (Roeper, 2013). Orexin A injection into the VTA increases cocaine- and morphine-related reward processing (Mahler et al., 2012), and intra-SN injection of orexin A induces hyperlocomotion and stereotypic behaviors (Liu et al., 2018; Nakamura et al., 2000). On the other hand, systemic injection of dopamine receptor antagonists reduces orexin A-induced increase of hyperlocomotion, stereotypic and grooming behaviors (Nakamura et al., 2000). However, whether the above effects of orexin signaling in the VTA and SN is mediated by dopaminergic or non-dopaminergic cells is not clear yet.

The orexin system consists of the two peptides orexin A and B, which are derived from the precursor, prepro-orexin (de Lecea et al., 1998; Sakurai et al., 1998). Both are endogenous ligands for two G-protein-coupled receptors, orexin receptor subtype 1 (Ox1R), and 2 (Ox2R) (Sakurai et al., 1998). Orexin A activates both receptors, while orexin B predominantly activates Ox2R (Sakurai et al., 1998). The mRNA detection by *in situ* hybridization revealed the expression of both receptors in VTA and SN (Marcus et al., 2001). However, the cell-type specific expression of Ox1R and Ox2R in the VTA and SN is not well understood. Electrophysiological studies showed that orexin receptors are present in

64 dopaminergic VTA neurons (Baimel et al., 2017; Korotkova et al., 2003; Tung et al., 2016), whereas
65 data for the SN seem controversial (Korotkova et al., 2002; Liu et al., 2018).

66 Here, we aim to map the expression patterns of Ox1R and Ox2R in dopaminergic VTA and SN
67 neurons and investigate the functional role of Ox1R using conditional knockout mice.

68 **Results**

69 **Ox1R is the predominant orexin receptor in dopaminergic neurons**

70 To analyze the expression patterns of orexin receptors in dopaminergic VTA and SN neurons, we
71 performed fluorescent *in situ* hybridization (RNAscope) of tyrosine hydroxylase (*Th*), Ox1R (*Hcrtr1*)
72 **Figure 1** with 2 supplements

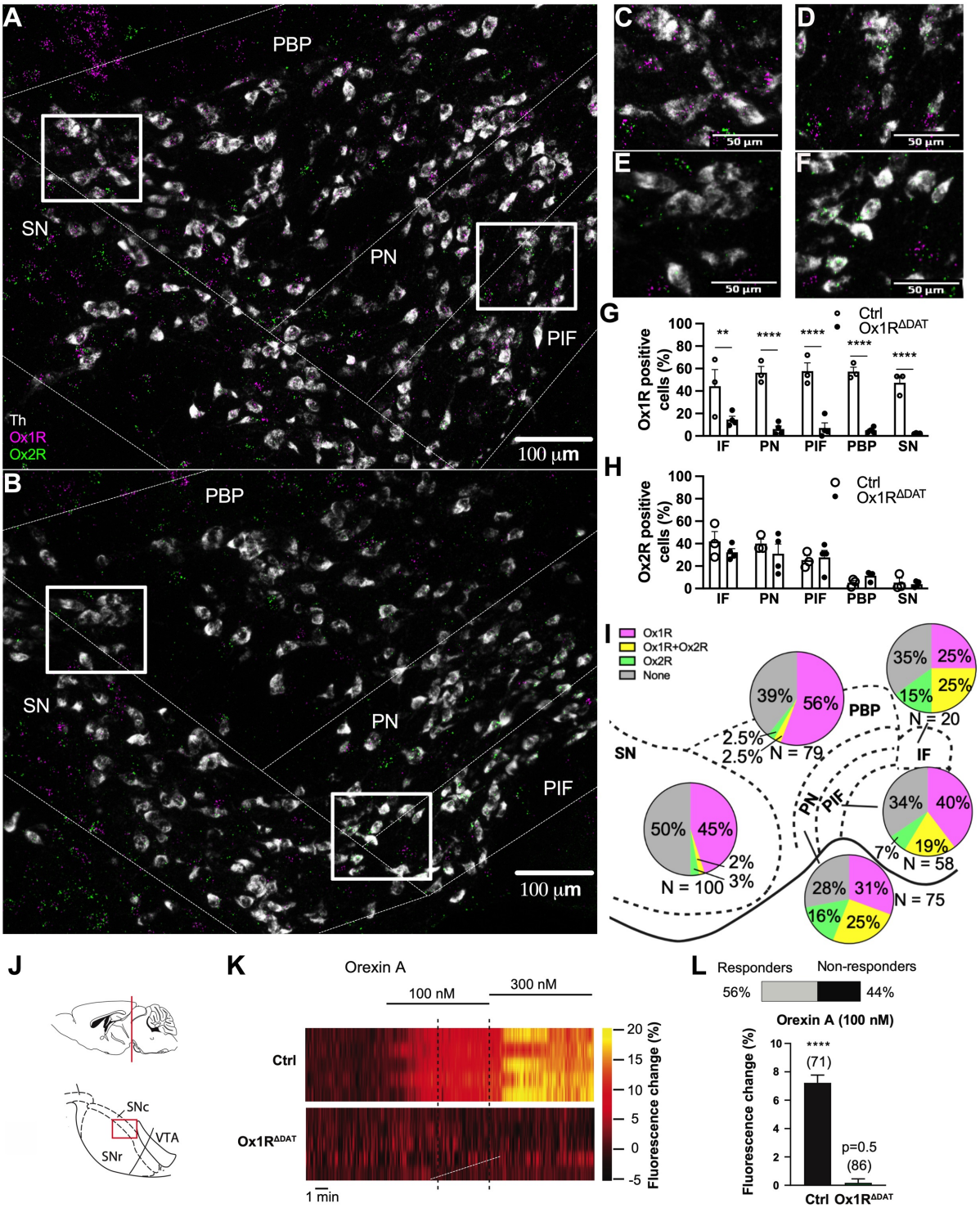

73

Figure 1. Ox1R predominantly mediates orexin-induced activation of dopaminergic neurons in the substantia nigra (SN).

Representative images of RNAscope *in situ* hybridization in SN and paranigral (PN), parainterfascicular (PIF) and parabrachial (PBP) subnuclei of the ventral tegmental area (VTA), of **(A)** a control and **(B)** an $Ox1R^{\Delta DAT}$ mouse. Amplifications of the **(C)** left and **(D)** right marked areas in white squares in (A). Amplifications of the **(E)** left and **(F)** right marked area in white squares in (B). White, tyrosine hydroxylase (Th); magenta, Ox1R; green, Ox2R. Scale bar: 100 µm (A, B) or 50 µm (C-F). Representative images of an overview in SN and VTA were shown in figure 1—figure supplement 1. Percentages of **(G)** Ox1R and **(H)** Ox2R positive neurons in Th positive neurons. IF, interfascicular subnuclei of VTA. Control, n = 3; $Ox1R^{\Delta DAT}$, n = 4. Data are represented as means ± SEM. **$p < 0.01$; ****$p < 0.0001$; as determined by two-way ANOVA followed by Sidak's post hoc test. **(I)** Schematic illustration of Ox1R and Ox2R expression in dopaminergic neurons in the VTA and SN. 3 control mice were analyzed and N indicates the mean dopaminergic neuron numbers in the respective subregions. Magenta, dopaminergic neurons only expressing Ox1R; green, dopaminergic neurons only expressing Ox2R; yellow, dopaminergic neurons expressing both Ox1R and Ox2R; grey, dopaminergic neurons expressing neither Ox1R or Ox2R. **(J-L)** Effect of orexin A on dopaminergic SN neurons analyzed by Ca^{2+} imaging with GCaMP6. Recordings were performed in brain slices from control and $Ox1R^{\Delta DAT}$ male mice with GCaMP6 expressed in dopaminergic SN neurons for Ca^{2+} imaging. **(J)** Schematic illustration of the SN. The red frame indicates the region where calcium imaging was performed. **(K, L)** Orexin A effect on $[Ca^{2+}]_i$ of dopaminergic SN neurons. **(K)** Heat maps of 5 individual dopaminergic SN neurons from control (top) and $Ox1R^{\Delta DAT}$ mice. The recordings show the responses to 100 nM orexin A. The dashed lines indicate the range where the responses were quantified. **(L)** Mean Ca^{2+} responses upon 100 nM orexin A application. Data are shown as the percentage of the maximal response to high K^+ saline. Bar graphs represent means ± SEM. The stacked bar shows the percentage of individual dopaminergic neurons in control mice in which the increase in $[Ca^{2+}]_i$ was larger than 3 x SD of the control, thus defining them as orexin A responsive (see Materials and Methods). The significance of mean changes in $[Ca^{2+}]_i$ during orexin A application were compared using one-sample t-tests. **** $p < 0.0001$. n values are given in brackets.

and Ox2R (*Hcrtr2*) in control (Ox1R flox/flox, DAT wt/wt) mice and $Ox1R^{\Delta DAT}$ (Ox1R fl/fl, DAT-Cre tg/wt) mice, from the same breeding crossing mice carrying a loxP-flanked Ox1R-allele (Ox1R fl/fl) with DAT-Cre mice (Ekstrand et al., 2007).

In control mice, Ox1R was expressed in 44 - 58% of dopaminergic neurons in all VTA and SN sub-regions, including the interfascicular (IF), paranigral (PN), parainterfascicular (PIF) and parabrachial (PBP) subnuclei of the VTA and SN. In contrast, Ox2R-positive dopaminergic neurons were mainly located in the medial VTA, including IF, PN, and PIF, with 25 to 42% of dopaminergic neurons expressing the Ox2R (Figure 1A, C, D, G, H; Figure 1—figure supplement 1A). While the above data were calculated as the mean percentages in the investigated mice, we also calculated the mean dopaminergic neuron numbers, separately for those expressing both or exclusively one of the

113 orexin receptor types. Thus, we could analyze the distribution of Ox1R-, Ox2R-, Ox1R and Ox2R-, and
114 none (of orexin receptors)-expressing dopaminergic neurons in each VTA subregions and SN, which
115 was shown in the schematic illustration with pie charts (Figure 1I). It showed similar results to the above:
116 47 - 59% of dopaminergic neurons expressed Ox1R in all VTA and SN sub-regions, and Ox2R was
117 mainly expressed by 26 - 41% of dopaminergic neurons in the medial VTA (Figure 1I). 19 - 25% of
118 dopaminergic neurons in the medial VTA expressed both Ox1R and Ox2R (Figure 1I). Of note,
119 abundant Ox1R and Ox2R expression was present in Th-negative neurons in the VTA and SN and
120 neighboring regions (Figure 1A, C, D, Figure 1—figure supplement 1A).

121 Since the vast majority of dopaminergic neurons express Ox1R, we focused on the functional
122 analysis of Ox1R signaling in dopaminergic neurons. Ox1R was specifically inactivated in
123 dopaminergic (DAT-expressing) neurons of mice ($Ox1R^{\Delta DAT}$). In $Ox1R^{\Delta DAT}$ mice, Ox1R expression in
124 dopaminergic neurons was significantly reduced and remained unchanged in Th-negative cells. In
125 contrast, the Ox2R expression patterns remained similar to that in the control mice, indicating the
126 successful and specific knockout of Ox1R in dopaminergic neurons (Figure 1B, E-H; Figure 1—figure
127 supplement 1B). To test if orexin activates dopaminergic SN neurons and to functionally validate the
128 deletion of Ox1R signaling, we performed Ca^{2+} imaging on dopaminergic SN neurons from control and
129 $Ox1R^{\Delta DAT}$ mice using the genetically encoded Ca^{2+} indicator GCaMP6 expressed in dopaminergic (DAT
130 expressing) neurons (Figure 1J-L, Figure1—figure supplement 2). During the experiments, GABAergic
131 and glutamatergic synaptic input was blocked. The orexin A-induced Ca^{2+} responses were expressed as
132 a percentage of the maximum fluorescence induced by KCl (Figure 1K, L, Figure1—figure supplement
133 2). Bath-applied 100 nM orexin A significantly increased $[Ca^{2+}]_i$ in dopaminergic SN control neurons
134 ($p < 0.0001$, $n = 71$, one-sample t-test). An analysis on the level of individual cells (3 sigma criterion)
135 showed that ~60% of dopaminergic SN neurons responded to 100 nM orexin A. In dopaminergic SN
136 neurons from $Ox1R^{\Delta DAT}$ mice, 100 nM orexin A had no effect ($p = 0.5$, $n = 86$, one-sample t-test) (Figure
137 1K, L).

138 In conclusion, Ox1R is the main orexin receptor expressed in dopaminergic VTA and SN
139 neurons and mediates their activation by orexin. Therefore, we wanted to determine further the
140 functional role of Ox1R signaling in dopaminergic neurons. By comparing data from control and

141 Ox1R$^{\Delta DAT}$ mice, we first identified behaviors modulated by orexin via dopaminergic neurons. In a
142 second step, we used PET imaging to define and map neuronal pathways modulated by orexin..

143 **Ox1R in dopaminergic neurons regulates novelty-induced locomotion and exploration**

144 The behavioral test included an analysis of locomotor behavior, novelty exploration, reward processing,
145 anxiety, and energy homeostasis. Since sex differences exist in orexin- and dopamine-mediated
146 behaviors (Durairaja & Fendt, 2020; Freeman et al., 2021; Lippert et al., 2020), we analyzed behavioral
147 **Figure 2** with 5 supplements

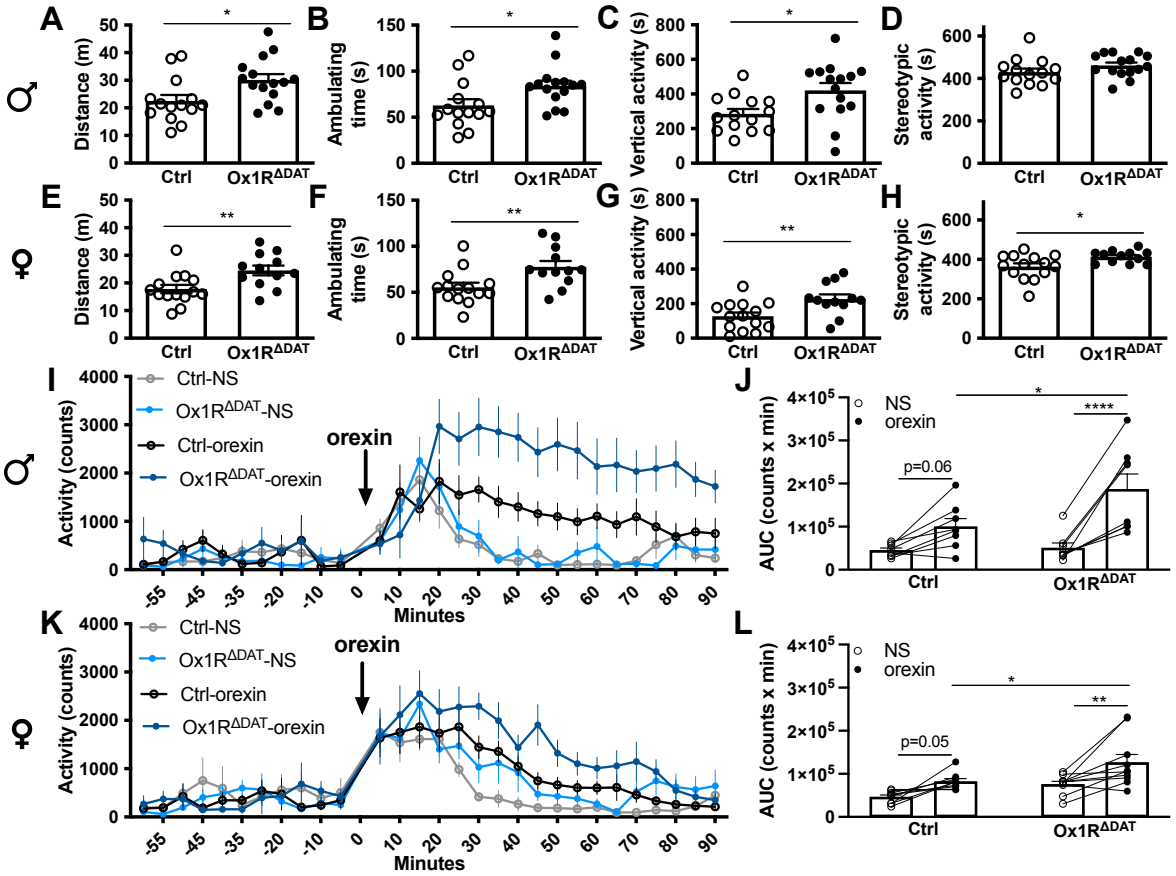

148

149 **Figure 2. Deficiency of Ox1R in dopaminergic neurons increases locomotion and exploration**
150 **behaviors.**
151 **(A)** Total traveling distance, **(B)** ambulating time, **(C)** vertical activity and **(D)** stereotypic activity of
152 male mice in the open field test. Control, n = 14; Ox1R$^{\Delta DAT}$, n = 15. **(E)** Total traveling distance, **(F)**
153 ambulating time, **(G)** vertical activity and **(H)** stereotypic activity of female mice in the open field test.
154 Control, n = 14; Ox1R$^{\Delta DAT}$, n = 12. Locomotor activity upon intracerebroventricular (ICV) injection of
155 saline (NS) or orexin A in **(I)** male and **(K)** female control and Ox1R$^{\Delta DAT}$ mice. **(J, L)** Quantification of
156 the area under curve (AUC) after orexin injection to (J) male and (L) female mice. Male, n = 8; female-
157 control, n = 9; female-Ox1R$^{\Delta DAT}$, n = 10. Data are represented as means ± SEM. *$p < 0.05$; **$p < 0.01$;
158 ****$p < 0.0001$; as determined by unpaired two-tailed Student's t-test (A-C, E-H), or two-way ANOVA
159 followed by Sidak's post hoc test (J, L).
160

161 phenotypes in both males and females. Compared to controls, Ox1R$^{\Delta DAT}$ mice did not show significant
162 changes in spontaneous locomotor activity in home cages (Figure 2—figure supplement 1). When
163 exposed to a novel open field, both male and female Ox1R$^{\Delta DAT}$ mice exhibited an increase in locomotion
164 and exploration, with increased traveling distance, ambulating time, and vertical activity in the open
165 field test (Figure 2A-C, E-G). Female Ox1R$^{\Delta DAT}$ mice also showed increased stereotypic activity (Figure
166 2D, H). Furthermore, intracerebroventricular (ICV) injection of orexin A (1 nmol) induced a more
167 pronounced increase of locomotor activity in both female and male Ox1R$^{\Delta DAT}$ mice, compared to control
168 mice (Figure 2I-L).

169 In a hole-board test, female Ox1R$^{\Delta DAT}$ mice showed increased nose pokes into the holes in early
170 (1st and 2nd) sessions compared to control mice (Figure 2—figure supplement 2B). This effect
171 disappeared later when mice became familiar with the environment (3rd – 8th session) (Figure 2—figure
172 supplement 2B). In the novel object recognition test, female Ox1R$^{\Delta DAT}$ mice spent more time with each
173 of the two identical objects in an open field compared to control mice (Figure 2—figure supplement 2E).
174 One hour later, when female mice were exposed to the same environment except that one object was
175 replaced by a novel object, there was no significant difference between control and Ox1R$^{\Delta DAT}$ mice in
176 exploring the novel object (Figure 2—figure supplement 2F). In contrast, male Ox1R$^{\Delta DAT}$ mice did not
177 behave differently in the hole-board and novel object recognition tests from controls (Figure 2—figure
178 supplement 2A, C, D). This indicates that Ox1R signaling in dopaminergic neurons is more important
179 for females in novelty-induced exploration, which was independent of novel object discrimination.

180 The behavioral changes seemed not related to alterations in anxiety, since there were no
181 detectable changes in anxiety-related behaviors in an open field test, dark/light box test or 0-maze test
182 (Figure 2—figure supplement 3).

183 **Ox1R deletion in dopaminergic neurons did not change energy metabolism and reward processing**

184 The orexin and dopaminergic systems are well known to regulate energy metabolism and reward
185 processing (Howe & Dombeck, 2016; Inutsuka & Yamanaka, 2013; Narayanan et al., 2010; Palmiter,
186 2007; Tsujino & Sakurai, 2013). Therefore, we measured the impact of Ox1R deletion in dopaminergic
187 neurons on metabolism and reward-related behaviors. We found that, compared to control mice, neither
188 male or female Ox1R$^{\Delta DAT}$ mice showed significant changes in the two-bottle preference test (comparing

189 sweet solution and water drinking), conditional place preference test (comparing cocaine and saline
190 injection) or energy metabolism, including body weight, fat mass, respiratory exchanging ratio, energy
191 expenditure, feeding behaviors, glucose tolerance and insulin sensitivity (Figure 2—figure supplement
192 4 and 5).

193 **Ox1R in dopaminergic neurons regulates specific neural pathways under different conditions**

194 To explore and map the underlying neuronal pathways of the orexin-mediated behaviors unbiasedly,
195 we performed positron emission tomography (PET) imaging of control and Ox1R$^{\Delta DAT}$ mice upon ICV
196 injection of orexin A or saline (control).

197 **Figure 3** with 2 supplements

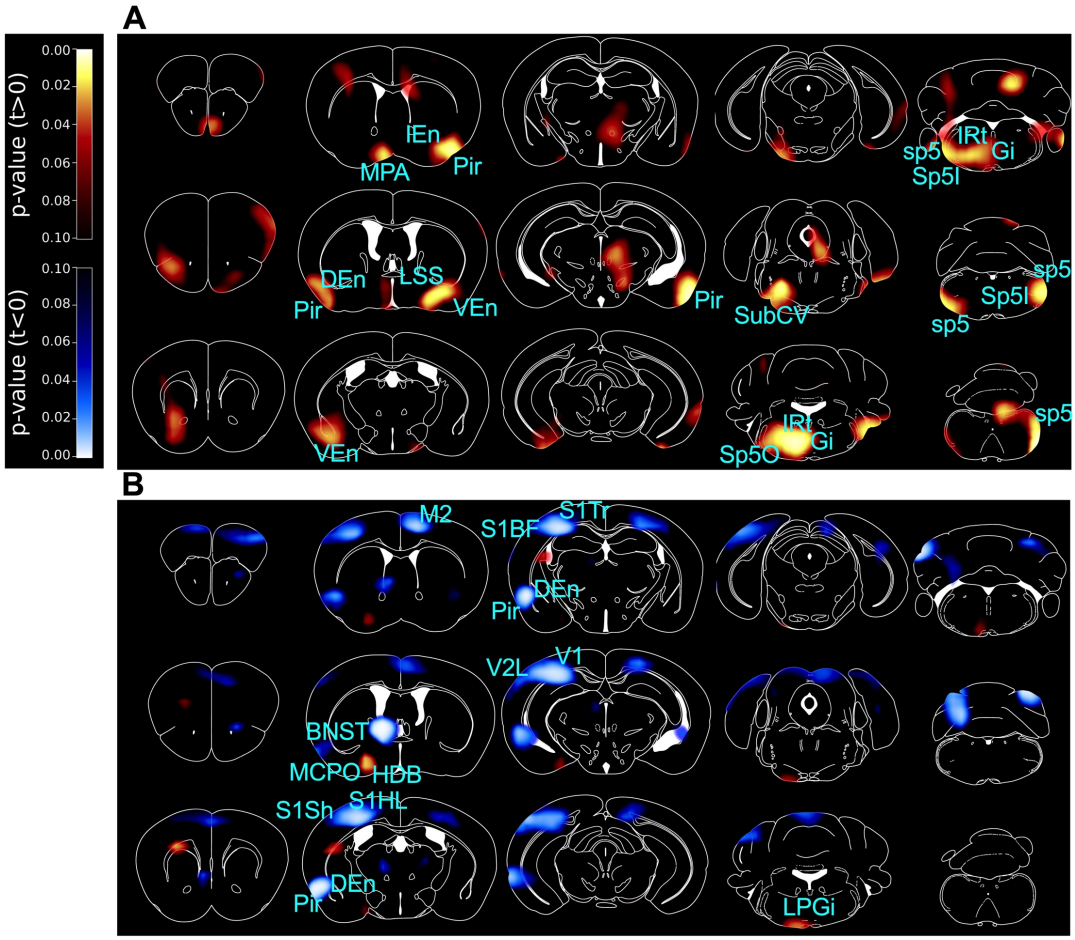

198

199 **Figure 3. PET imaging studies comparing Ox1R$^{\Delta DAT}$ and control mice.**
200 3D maps of p-values in PET imaging studies comparing Ox1R$^{\Delta DAT}$ and control mice, after
201 intracerebroventricular (ICV) injection of **(A)** saline (NS) and **(B)** orexin A. Brain areas with significant
202 changes are indicated. Control-NS, n = 8; control-orexin, n = 6; Ox1R$^{\Delta DAT}$, n = 8. M2, secondary motor
203 cortex; MPA, medial preoptic area; Pir, piriform cortex; IEn, intermediate endopiriform claustrum; DEn,
204 dorsal endopiriform claustrum; VEn, ventral endopiriform claustrum; LSS, lateral stripe of the striatum;

205 BNST, the dorsal bed nucleus of the stria terminalis; HDB, nucleus of the horizontal limb of the diagonal
206 band; MCPO, magnocellular preoptic nucleus; S1Sh, primary somatosensory cortex, shoulder region;
207 S1HL, primary somatosensory cortex, hindlimb region; S1BF, primary somatosensory cortex, barrel
208 field; S1Tr, primary somatosensory cortex, trunk region; V1, primary visual cortex; V2L, secondary
209 visual cortex, lateral area; SubCV, subcoeruleus nucleus, ventral part; Gi, gigantocellular reticular
210 nucleus; IRt, intermediate reticular nucleus; LPGi, lateral paragigantocellular nucleus; Sp5O, spinal
211 trigeminal nucleus, oral part; Sp5I, spinal trigeminal nucleus, interpolar part; sp5, spinal trigeminal tract.
212

213 In $Ox1R^{\Delta DAT}$ mice under control conditions (saline injection), we observed higher neuronal
214 activity around the medial preoptic area (MPA), piriform cortex (Pir), endopiriform claustrum, lateral
215 stripe of the striatum (LSS), ventral part of subcoeruleus nucleus (SubCV), spinal trigeminal nucleus,
216 spinal trigeminal tract (sp5), the intermediate reticular zone (IRt) and the gigantocellular reticular
217 nucleus (Gi) than control mice (Figure 3A, Figure 3—figure supplement 1). Compared to control mice,
218 central application of orexin (1 nmol, ICV) to $Ox1R^{\Delta DAT}$ mice induced higher neuronal activity around
219 the lateral paragigantocellular nucleus (LPGi), nucleus of the horizontal limb of the diagonal band
220 (HDB) and magnocellular preoptic nucleus (MCPO), and lower activity around secondary motor cortex
221 (M2), the dorsal bed nucleus of the stria terminalis (BNST), the hindlimb, shoulder, and trunk regions
222 and barrel field of primary somatosensory cortex (S1HL, S1Sh, S1Tr, and S1BF), the lateral area of
223 secondary visual cortex (V2L), primary visual cortex (V1), Pir and dorsal endopiriform claustrum (DEn)
224 (Figure 3B, Figure 3—figure supplement 1). PET imaging did not reveal significant changes in the VTA
225 and SN (Figure 3).

226 Postmortem analysis of c-Fos staining revealed low c-Fos expression in dopaminergic neurons
227 in the VTA and SN. In contrast, clear orexin-induced c-Fos activity was observed in non-dopaminergic
228 cells (Figure 3—figure supplement 2). Further studies would be needed to investigate how orexin
229 directly and indirectly affect the VTA and SN neurons in the brain.

230 **Dopamine receptors in the dorsal BNST and LPGi**

231 Based on the PET imaging findings, we analyzed the dopaminergic pathways into the dorsal BNST and
232 LPGi that could have been affected by the Ox1R. To this end, we injected Cre-dependent AAV-EYFP
233 bilaterally into the VTA and SN of DAT-Cre (DAT^{EYFP}) and $Ox1R^{\Delta DAT}$ ($DAT^{\Delta Ox1R;\ EYFP}$) mice, and
234 discovered dopaminergic projections in the dorsal BNST and LPGi (Figure 4—figure supplement 1),
235 suggesting that VTA and SN dopaminergic neurons could directly modulate neuronal activity in the

236 dorsal BNST and LPGi. To further explore this idea, we assessed expression of Fos and dopamine

237 receptors in the dorsal BNST and LPGi by immunostaining and RNAscope experiments.

238 **Figure 4** with 1 supplement

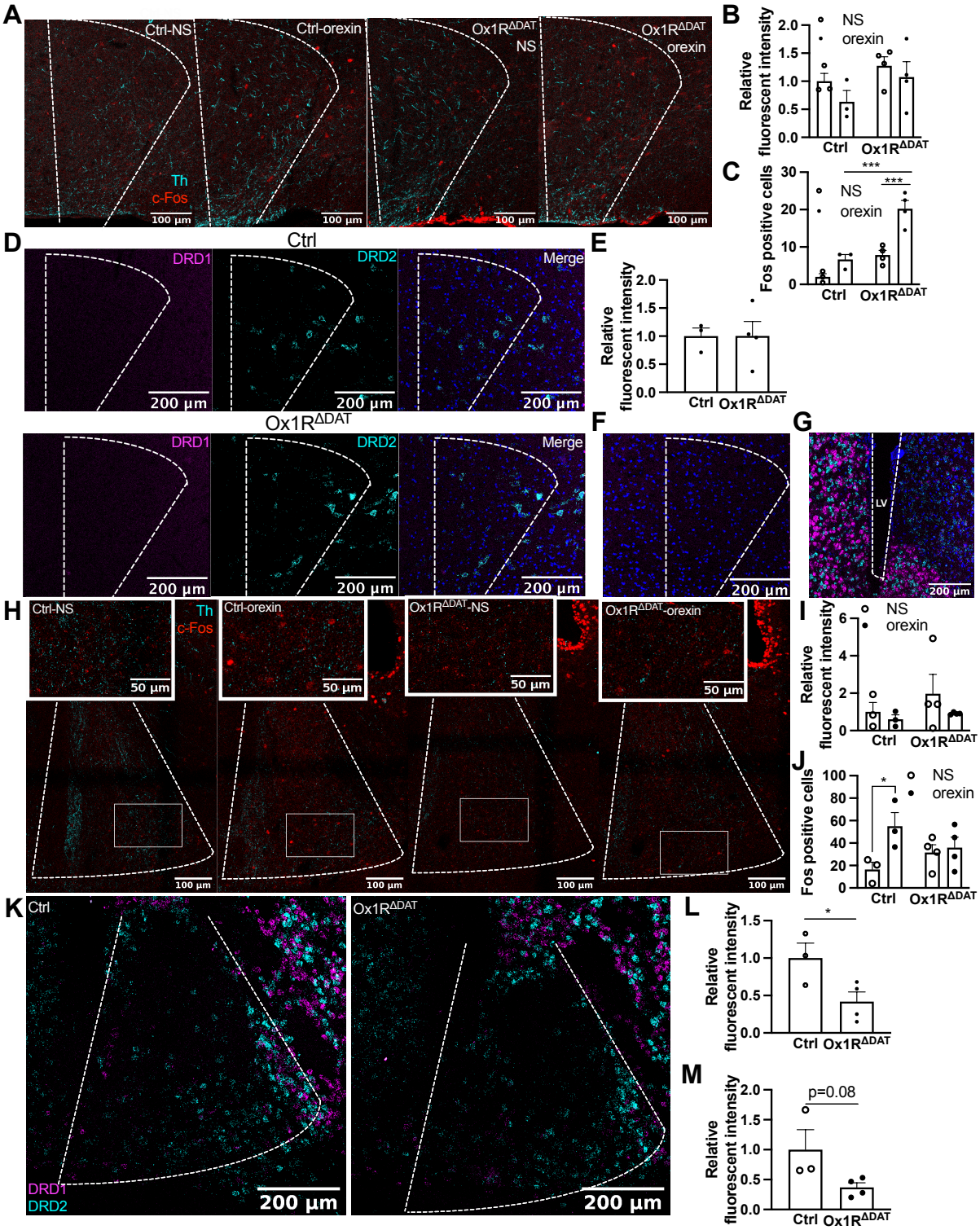

239

240 **Figure 4. c-Fos and dopamine receptors in the lateral paragigantocellular nucleus (LPGi) and the**

241 **dorsal bed nucleus of the stria terminalis (BNST).**

242 **(A)** Representative images of c-Fos and tyrosine hydroxylase (Th) staining in LPGi of control and
243 $Ox1R^{\Delta DAT}$ mice injected (ICV) with saline (NS) and orexin A. Quantification of **(B)** Th fluorescence
244 and **(C)** c-Fos positive neurons in LPGi. **(D)** Representative images of D1 and D2 subtypes of dopamine
245 receptor (DRD1 and DRD2) in LPGi of control and $Ox1R^{\Delta DAT}$ mice. **(E)** Quantification of DRD2
246 fluorescence in LPGi. **(F)** Representative images of a negative control staining of DRD1 and DRD2 in
247 LPGi of control mice, and **(G)** a positive control staining around the lateral ventricle (LV). **(H)**
248 Representative images of c-Fos and Th staining in the dorsal BNST of control and $Ox1R^{\Delta DAT}$ mice
249 injected (ICV) with saline or orexin A. Quantification of **(I)** Th fluorescence and **(J)** c-Fos positive
250 neurons in dorsal BNST. **(K)** Representative images of DRD1 and DRD2 in the dorsal BNST of control
251 and $Ox1R^{\Delta DAT}$ mice. Quantification of **(L)** DRD1 and **(M)** DRD2 fluorescence in dorsal BNST. Scale
252 bar: 200 µm (D, F, G, K), 100 µm (A, H) or 50 µm (insertions in H). Control, n = 3; $Ox1R^{\Delta DAT}$, n = 4.
253 Cyan, Th; red, c-Fos (A, H). Magenta, DRD1; cyan, DRD2; blue, dapi (D, F, G, K). Data are represented
254 as means ± SEM. *$p < 0.05$; ***$p < 0.001$; as determined by unpaired two-tailed Student's t-test (L, M),
255 or two-way ANOVA followed by Sidak's post hoc test (C, J).
256
257 Orexin injection (1 nmol, ICV) induced higher c-Fos expression levels in LPGi of male
258 $Ox1R^{\Delta DAT}$ mice compared to control mice (Figure 4A, C). Only the inhibitory D2 but not excitatory D1
259 subtypes of dopamine receptors (DRD2, DRD1) could be detected in LPGi (Figure 4D, E). Both
260 receptors were detected around the lateral ventricle (as positive control), whereas no signal was
261 detectable in LPGi incubated with negative control probe for mice (Figure 4F, G). Th-positive fibers
262 were detected in LPGi but not Gi (Figure 4A, B), consistent with previous reports (Kitahama et al.,
263 2000). These data support the hypothesis that Ox1R deletion in dopaminergic neurons results in the
264 disinhibition of dopaminergic signaling in LPGi.

265 Orexin injection increased c-Fos expression in the dorsal BNST in control but not in $Ox1R^{\Delta DAT}$
266 mice (Figure 4H, J). The expression of DRD1 was significantly reduced, and DRD2 expression levels
267 showed a tendency towards a decrease in dorsal BNST of $Ox1R^{\Delta DAT}$ mice (Figure 4K-M). The Th
268 expression levels were not changed between genotypes (Figure 4H, I). This indicates that dorsal BNST
269 could be less activated, due to the decrease of DRD1 and the lack of orexin-mediated activation of
270 dopaminergic neurons.

Discussion

The main findings of this study are based on RNAscope and optophysiological experiments. These data show that Ox1R is the most abundant orexin receptor in the midbrain and the only orexin receptor in the SN. Ca^{2+} imaging experiments on SN dopaminergic neurons from control and $Ox1R^{\Delta DAT}$ mice functionally confirm these results. They show that orexin-induced activation of SN dopaminergic neurons is exclusively mediated by Ox1R. In addition, the behavioral experiments, PET imaging and Fos analyses provide important evidence of these data's systemic relevance. They should serve as a basis for developing testable working hypotheses on the systemic physiological role of orexin signaling. Ox1R deficiency in DAT-expressing neurons causes an increase in novelty-induced locomotion and exploration without altering energy metabolism and anxiety- or reward-processing-related behaviors. PET imaging, and Fos and DRD expression analysis provide some indications about the underlying mechanisms.

Earlier studies showed that orexin-induced activation of VTA dopaminergic neurons (Baimel et al., 2017; Korotkova et al., 2003; Tung et al., 2016). At the end of whole-cell patch clamp recordings, mRNA measurement of the individual recorded VTA neurons revealed fewer Ox2R- than Ox1R-positive dopaminergic neurons (Korotkova et al., 2003), which is in line with our findings. While our data clearly show an orexin A-induced activation of dopaminergic SN neurons when GABAergic and glutamatergic synaptic input is blocked, previous *in vitro* (Korotkova et al., 2002) or *in vivo* electrophysiological recordings (Liu et al., 2018) studies were controversial about whether orexin A could activate dopaminergic neurons in the SN. Since Ox1R and Ox2R are expressed by non-dopaminergic neurons around the SN, recordings in the absence of synaptic blockers, could detect a mixed direct and indirect orexin-induced response in dopaminergic neurons (Nair-Roberts et al., 2008). This may partially explain their controversial findings.

We found that Ox1R deficiency in dopaminergic neurons caused an increase in novelty-induced locomotion and exploration, which could indicate elevated arousal levels and hyperactivity. Interestingly, children with attention deficit and hyperactivity disorder (ADHD) have lower orexin A but unaltered orexin B levels in plasma compared to the healthy controls (Baykal et al., 2019). ADHD patients exhibit impaired dopaminergic functions, and medicine improving dopaminergic signaling is

299 used to treat ADHD in clinics (Feldman & Reiff, 2014; Volkow & Swanson, 2013). Ox1R signaling in
300 dopaminergic neurons might be important to limit novelty-induced arousal and hyperactivity, which are
301 related to task performance and learning capability.

302 We did not observe significant impact of Ox1R signaling in dopaminergic neurons on reward
303 processing. Previous studies reported that Ox1R signaling in VTA promoted reward processing with
304 pharmacological methods (Tsujino & Sakurai, 2013). The difference could have resulted from the
305 involvement of non-dopaminergic neurons in VTA or different behavioral models. It would be
306 interesting to identify the effect under other conditions, such as obesity and operant reward learning, in
307 the future.

308 The PET imaging results suggest that Ox1R signaling in dopaminergic neurons affects separate
309 and distinct neuronal circuits, depending on the mode of stimulation. Orexin and dopaminergic systems
310 are known to increase arousal in mammals' sleep-wake transitions, locomotor activity, and motivation
311 (Berke, 2018; Berridge et al., 2010; Furlong et al., 2009; Mahler et al., 2014). The orexin system
312 responds to various environmental stimuli, such as stress and novelty (Berridge et al., 2010; Gonzalez
313 et al., 2016). Projection-defined dopaminergic populations in the VTA exhibited different responses to
314 orexin A (Baimel et al., 2017). Our PET imaging experiments, without orexin application, indicate that
315 Ox1R signaling in dopaminergic neurons modulates brain regions (MPA, Pir, endopiriform claustrum,
316 LSS, SubCV, spinal trigeminal nucleus, sp5, IRt and Gi) important for olfaction, eating, arousal and
317 sleeping (Supplementary table 1).When central orexin levels were increased by orexin injection, Ox1R
318 signaling in dopaminergic neurons regulates HDB, MCPO, Pir, DEn, S1, V2L, V1, BNST, LPGi and
319 M2, which are important for sensation, emotion, exploration, and action selection (Supplementary table
320 1). In future studies, it would be interesting to investigate the direct and indirect downstream pathways
321 of Ox1R-expressing dopaminergic neurons. Interestingly, in the fruitfly *Drosophila melanogaster*, it
322 has been shown that the dopaminergic system oppositely regulates sleep-wake arousal and
323 environmentally stimulated arousal, and the authors discussed the possibility to identify similar patterns
324 in mammals (Lebestky et al., 2009). It was further suggested that the dopaminergic system differentially
325 regulates arousal levels under different stimulating conditions (Lebestky et al., 2009; Lima &
326 Miesenbock, 2005).

327 We found a potential direct impact of dopaminergic neurons on LPGi and BNST. DRD1 and
328 DRD2 in the BNST regulate anxiety, fear, and addiction (De Bundel et al., 2016; Eiler et al., 2003;
329 Giardino et al., 2018; Krawczyk et al., 2013). LGPi regulates exploratory behaviors and locomotor speed
330 (Takatoh et al., 2013; Arber & Costa, 2022; Capelli et al., 2017). There are few publications on the
331 functional relevance of dopaminergic projections in the LPGi. Future studies would be very interesting
332 to functionally analyze DRD2 signaling in the LPGi and to understand how orexin- interacts with DRD2
333 signaling.

334 **Materials and Methods**

335 **Animal care**

336 All animal procedures were conducted in compliance with protocols approved by the local government
337 authorities (Bezirksregierung Cologne, Germany) and were in accordance with National Institutes of
338 Health guidelines. Mice were housed in groups of 3 - 5 at 22°C - 24°C using a 12-hr light/12-hr dark
339 cycle. Animals had *ad libitum* access to water and food at all times. Animals were fed a NCD (R/M-H,
340 ssniff^{R}), which contains 57% calories from carbohydrates, 34% calories from protein, and 9% calories
341 from fat.

342

343 **Generation of Ox1R$^{\Delta DAT}$ mice**

344 Mice carrying a loxP-flanked Ox1R-allele (Ox1R fl/fl) were generated in our facility (Xiao et al., 2021).
345 Ox1R fl/fl mice were crossed with Dat-Cre mice (Ekstrand et al., 2007) to obtain Ox1R fl/fl, Dat-Cre
346 tg/wt mice, i.e. dopaminergic-specific Ox1R knockout mice on a C57/Bl6 N background (Ox1R$^{\Delta DAT}$).
347 Mice from the same breeding without the Cre transgene were used as controls (Ox1R fl/fl, Dat-Cre
348 wt/wt).

349

350 **Glucose and insulin tolerance tests**

351 Glucose tolerance tests were performed on 12-weeks-old animals that had been fasted for 6 hours from
352 9 am. Insulin tolerance tests were performed on 11-weeks-old random-fed mice around 9 am. Animals
353 received an intraperitoneal injection of 20% glucose (10 ml/kg body weight; KabiPac) or insulin (0.75
354 U/kg body weight; Sanofi-Aventis) into the peritoneal cavity, respectively. Blood glucose values were
355 determined in whole venous blood using an automatic glucose monitor (Contour^{R}, Bayer). Glucose
356 levels were determined in blood collected from the tail tip immediately before and 15, 30, and 60
357 minutes after the injection, with an additional value determined after 120 minutes for the glucose
358 tolerance tests.

359

360 **Analysis of body composition**

361 Nuclear magnetic resonance (NMR) was employed to determine whole body composition of live
362 animals on NCD at the age of 20 weeks using the NMR Analyzer minispec mq7.5 (Bruker Optik,
363 Ettlingen, Germany).
364
365 **Histology**
366 Brains from male mice were removed, post-fixed in 4% paraformaldehyde (PFA) for the indicated time,
367 and dehydrated in 20% sucrose in 0.1M phosphate-buffered saline (PBS) overnight. Brains were stored
368 at -80°C until cutting.
369 **Immunostaining**
370 Brains were post-fixed for 6 h at 4 °C and cut (30 µm) with Leica CM3050 S Research Cryostat. Sections
371 were incubated in 0.3% glycine for 10 min after washing in 0.1 M PBS for 2 × 10 min. After washing
372 in PBS for another 10 min, sections were incubated in 0.03% SDS (in PBS) for 10 min before they got
373 blocked with 3% donkey serum (in PBS, 0.25% Triton X-100) for 1 h at RT. Afterwards, they were
374 incubated with primary antibodies, including goat anti-c-Fos (sc-526, Santa Cruz Biotechnology),
375 chicken anti-GFP (ab13970, Abcam) and/or rabbit anti-Th (ab112, Abcam), for overnight (GFP) or 48
376 h (c-Fos and Th) at 4°C, washed in PBS for 3 × 10 min, and incubated with secondary antibodies,
377 including Alexa Fluro 594 donkey anti-goat, FITC donkey anti-chicken, Alexa Fluro 488 donkey anti-
378 rabbit (a11058, sa 1-7200 and a21206, Invitrogen), for 1 h at RT. After washing in PBS for 3 × 10 min,
379 slices were mounted and covered with VECTASHIELD Antifade Mounting Medium with DAPI (Vector
380 Laboratories). Slices were stained together at one time for each experiment to have identical conditions
381 for comparable signals. Slides were stored at 4 °C until imaging. Images were obtained with confocal
382 laser scanning microscope Leica TCS SP8 and manually analyzed with Image J/FIJI (version 1.50d).
383 **RNAscope fluorescent in situ hybridization**
384 Brains from 12-wk-old male mice were post-fixed for 20 - 22 h at RT and cut (20 µm). Slides were
385 stored at -80°C until staining. All reagents were purchased from Advanced Cell Diagnostics, and the
386 staining was performed with the RNAscope Multiplex Fluorescent v2 kit (ACD, Advanced Cell
387 Diagnostics) according to the user manual. Probes for Ox1R (*Hcrtr1*, 471561-C3, ACD) and Ox2R
388 (*Hcrtr2*, 471551, ACD), DRD1 (*Drd1a*, 406491-C2, ACD), DRD2 (*Drd2*, 406501), and Th (*Th*,

389 317621-C4) were purchased from ACD. In brief, slides were briefly washed in diethyl-pyrocarbonate
390 (DEPC)-treated Millipore water, air dried, and then dried at 60°C overnight. On the second day, slides
391 were treated with hydrogen peroxide (H_2O_2) for 10 min at RT, washed in water, and boiled in Target
392 Retrieval solution (around 99.4 °C) for 8 -10 min. After a brief washing in water and dehydration in
393 absolute ethanol, slides were incubated with protease IV for 30 min at RT. Slides were washed again in
394 water and hybridized with the mixture of probes in different channels for 2 h in a humidified chamber
395 at 40 °C. Afterwards, the hybridization was amplified with AMP 1 for 30 min, AMP 2 for 30 min and
396 AMP 3 for 15 min. The signal was then developed for each channel. For example, for channel 1, slides
397 were incubated with HRP-C1 for 15 min, the fluorophore for 30 min, and HRP blocker for 15 min. All
398 amplification and development were performed at 40 °C, and 2 × 2 min of washing in ACD wash buffer
399 was performed after each step. Finally, the slides were counterstained with DAPI for 1 min, mounted
400 with Prolong™ Gold Antifade reagent with DAPI (Invitrogen), and covered with coverslips.
401 Slides were dried and stored at 4 °C. Imaging was performed with a confocal laser scanning
402 microscope Leica TCS SP8. The images were manually analyzed with Image J/FIJI (version 1.50d).
403
404 **<u>Ca^{2+} imaging</u>**
405 Calcium dynamics were measured in dopaminergic substantia nigra neurons using the genetically
406 encoded calcium indicator GCaMP6. Experiments were performed on brain slices from 18-19 week-old
407 male control and $Ox1R^{\Delta DAT}$ mice. A minimum of 4 weeks separated the GCaMP6 virus injection and
408 the imaging experiments. Animals were kept under standard laboratory conditions, with tap water and
409 chow available ad libitum, on a 12h light/dark cycle. The animals were lightly anesthetized with
410 isoflurane (B506; AbbVie Deutschland GmbH and Co KG, Ludwigshafen, Germany) and decapitated.
411 Coronal slices (280 µm) containing SN were cut with a vibration microtome (VT1200 S; Leica,
412 Germany) under cold (4°C), carbogenated (95% O_2 and 5% CO_2), glycerol-based modified artificial
413 cerebrospinal fluid (GaCSF). GaCSF contained (in mM): 244 Glycerol, 2.5 KCl, 2 $MgCl_2$, 2 $CaCl_2$, 1.2
414 NaH_2PO_4, 10 HEPES, 21 $NaHCO_3$, and 5 Glucose adjusted to pH 7.2 with NaOH. The brain slices were
415 continuously superfused with carbogenated aCSF at a flow rate of ~2.5 $ml \cdot min^{-1}$. aCSF contained (in
416 mM): 125 NaCl, 2.5 KCl, 2 $MgCl_2$, 2 $CaCl_2$, 1.2 NaH_2PO_4, 21 $NaHCO_3$, 10 HEPES, and 5 Glucose

417 adjusted to pH 7.2 with NaOH. To reduce GABAergic and glutamatergic synaptic input the aCSF
418 contained 10^{-4} M PTX (picrotoxin, P1675; Sigma-Aldrich), 5 x 10^{-6} M CGP (CGP-54626 hydrochloride,
419 BN0597, Biotrend), 5 x 10^{-5} M DL-AP5 (DL-2-amino-5-phosphonopentanoic acid, BN0086, Biotrend),
420 and 10^{-5} M CNQX (6-cyano-7-nitroquinoxaline-2,3-dione, C127; Sigma-Aldrich).

421 The imaging setup consisted of a Zeiss AxioCam/MRm CCD camera with a 1388x1040 chip
422 and a Polychromator V (Till Photonics, Gräfelfing, Germany) that was coupled via an optical fiber into
423 the Zeiss AxioExaminer upright microscope (Objective W "Plan-Apochromat" 20x/1.0 DIC D=0.17
424 M27 75mm). The camera and polychromator were controlled by the software Zen pro, including the
425 module 'Physiology' (2012 blue edition, Zeiss). The SN neurons were identified according to their
426 anatomical location and expression of the GCaMP6. Calcium signals in GCaMP6 expressing cells were
427 monitored by images acquired at 470 nm excitation wavelengths with 20 ms exposure time at ~0.2 Hz.
428 The emitted fluorescence was detected through a 500-550 nm bandpass filter (BP525/50), and data were
429 acquired using 4x4 on-chip binning. Images were recorded in arbitrary units (AU) and analyzed as 16-
430 bit grayscale images.

431 Orexin A (ab120212, Abcam) in the concentration of 100 nM was applied for 8 min. To analyze
432 the orexin effect, we compared the fluorescence measured during 4 min intervals that were recorded
433 immediately before and at the end of the peptide application. This protocol was followed by applying
434 high K^+ concentration saline (40 mM KCl; osmolarity was adjusted by reducing the NaCl concentration
435 accordingly) to elicit the maximal calcium response.

436 The image analysis was performed offline using Image J (version 1.53a), Igor Pro 6
437 (WaveMetrics, USA), and Prism 8 (GraphPad, California, USA). After the experiments, regions of
438 interest (ROI) were defined based on the high K^+ saline responses. The mean AU values of the ROIs
439 were calculated in Image J. Time series analysis was performed with Igor Pro 6. To correct for bleaching
440 artifacts, the baseline fluorescence (without orexin application) was fit. The extended fit was subtracted
441 from the raw data. The orexin-induced Ca^{2+} signals were normalized to the high (40 mM) K^+ response.
442 On the single-cell level, a neuron was considered orexin-responsive if the change in fluorescence
443 induced by orexin was 3 times larger than the standard deviation (SD) (3 sigma criterion) of the baseline
444 fluorescence.

445 **Food intake and spontaneous activity**

446 Mice (20 weeks old) were analyzed for food intake, spontaneous activity, respiratory exchanging ratio
447 and energy expenditure in a PhenoMaster System (TSE Systems) as previously described (Jordan et al.,
448 2011).

449

450 **Behavioral studies**

451 Mice were moved into the behavioral test room, weighed, and handled 1 week before the measurement.
452 On the day of the tests, mice (9-15 weeks old) were moved near to the equipment and handled 1 h before
453 the tests. There was a 1-week break between different behavioral tests for anxiety, exploration or
454 locomotion when using the same mice.

455 **Open field test (OFT)， dark/light (D/L) box and Hole-board tests**

456 OFT and D/L box tests were performed with a Seamless Open Field Starter Package for Mouse plus the
457 Light/Dark Insert or the hole-board floor (Med Associates, Inc.) between 10 am to 4 pm.

458 To start OFT, mice were put in the middle of a clear Plexiglas® chamber (27.3 cm × 27.3 cm ×
459 20.3 cm) sitting in a sound-attenuating cubicle, and mouse movement was automatically traced for 30
460 min with 48 infrared beams divided into the X, Y and Z plane. For the D/L box test, a black Plexiglas®
461 box (half the size of the chamber) was inserted at the left side of the chamber, with an opening at the
462 middle side. Mice were put in the middle of the light side and faced the openings. Mouse movement
463 was traced for 5 min. For the hole-board test, a metal hole-board floor with 16 equally spaced holes for
464 exploration was inserted in the chamber. Mice were put in the middle of the chambers and the nose
465 pokes were monitored automatically for 10 min per session. There was 1 h break between each session.
466 4 sessions per day were analyzed for 2 consecutive days.

467 **Elevated 0-maze test**

468 An elevated 0-maze test was performed with TSE elevated 0-Maze in combination with the video
469 tracking system TSE VideoMot 3D version 7.01. There are 2 closed and 2 open runways without a
470 center position. The outer diameter is 48 cm, the arm width is 5 cm, the wall height is 10 cm and the
471 base height is 55 cm. Mice were put in the middle of an open arm and faced to the closed arm to start
472 the experiment. Mouse movement was monitored for 5 min.

473 **Novel object recognition test**

474 Novel object recognition test was modified from the publication before (Ruud et al., 2019). The mouse
475 was acclimated and measured for 10 min in the 1st session and for 5 min in the 2nd session on the same
476 day, in a polycarbonate box with non-transparent walls (50 cm × 50 cm × 30 cm). Two objects were
477 present in the box. In the 1st session, two identical objects (glass beaker filled with blue marbles) were
478 present and fixed with odor-free adhesive to the ground flooring at two sides of the box delineated
479 diagonally. In each diagonal corner, the object is 11.5 cm and 14 cm from each wall respectively, and
480 the distance between the two objects is 17.5 cm. Mice always started at the same corner which was
481 between the two fixed objects and were allowed to explore and learn the experimental area and objects.
482 In the 2nd session which started after a 1-h break in the home cage, one of the two identical objects was
483 replaced with a novel object (Lego® Primo brick), and mice were allowed again to explore the
484 environment and objects. The positions of the mouse nose, tail and center were monitored with a video
485 tracking system TSE VideoMot 2. The interaction with a fixed object was identified when the nose was
486 facing the object within a distance of 2 cm.

487 **Conditioned place preference test for cocaine**

488 The test was modified from previous publication (Ruud et al., 2019), and was performed in a
489 polycarbonate box with non-transparent walls. The box was separated into 3 compartments with 2
490 independent partitions. It contains a left compartment with zebra stripes (white and black) painted on
491 the wall and a rough ground (16.5 x 13.2 x 21.2 cm), a small middle area (7.0 x 13.2 x 21.2 cm), and a
492 right compartment with a white wall and smooth ground. Mouse movement was monitored with TSE
493 VideoMot 2 for 30 min per session, 1 session per day. Mice started from the middle area and had access
494 to both left and right compartments through an opening (4.0 cm x 4.2 cm) in the partition during the
495 habituation and pre-test days (d1-3) and on the test day (d10), and were put into and kept in either the
496 left or right compartment without an opening in the partition during the conditioning phase (d4-9). The
497 preference of the two compartments by nature was analyzed during the pre-test days. At the conditioning
498 phase, on alternative days, mice received i.p. injection of cocaine (5 mg/kg BW) or saline immediately
499 before entering the respective compartments. Cocaine and saline were always paired to the non-
500 preferred and preferred compartments, which were determined by pre-tests, respectively. There was no

501 injection on the habituation, pre-test or test days. The percentage of time spent in the reward-paired
502 compartment was calculated: 100 x time spent in the compartment / (total time - time spent in the middle
503 area). The CPP score was then analyzed using the calculated percentage of time: 100 x (time on the test
504 day – time on pre-test days)/ time on pre-test days.

505 **Sucrose/sucralose preference test**

506 Two-bottle tests were performed with 2 15-ml falcon tubes connected to sippers. Mice were single caged
507 1 week before the beginning of the experiment. 2 falcon tubes filled with water (side-by-side) replaced
508 the normal water bottle. Water intake was monitored for a week to make sure mice adjusted to drinking
509 from the sippers. When the test started, 2 new sipper tubes of water were used for 2 days of baseline
510 measurement and were then replaced with one containing water and one containing sucrose/sucralose
511 solution for 2 days of preference measurement. Animals received a 0.5%, 1% and 2% (w/v) sucrose
512 solution and 1 mM sucralose solution in sequential. Between the preference tests of different solutions,
513 2 days of baseline measurement were performed with 2 new sipper tubes of water as a washout. To
514 avoid side bias, the positions of 2 sipper tubes were switched every day, with the sucrose/sucralose tube
515 always starting on the non-preferred position, which was determined by water intake on the day before
516 the preference measurement. Sipper tubes were weighed every day.

517

518 **<u>ICV cannula implantation and injection</u>**

519 12-wk-old mice received 1 mg/ml of tramadol in drinking water 2 d before the surgeries. On the day of
520 surgery, mice were anesthetized with isoflurane, and a bolus of buprenorphine (0.1 mg/kg BW) was
521 given (i. p.) to reduce pain. Brain regions were identified according to the atlas (Franklin & Paxinos,
522 2007). After alignment of the brain in the stereotaxic surgery platform, one small hole was drilled in the
523 skull and the ICV cannula (26 gauge, Plastics One) was immediately implanted (AP: -0.2 mm, ML: +1
524 mm, DV: -2.4 mm) and fixed to the skull with dental acrylic (Super-Bond C&B). The dummy cannula
525 caps were inserted to close and protect the cannula. Mice received a bolus of meloxicam (5 mg/kg BW,
526 s.c.), and tramadol in drinking water for 3 d after surgeries to relieve pain. BW was checked twice a
527 day. Experiments started at least 1 week later. For injection, the catheter was attached to an injector
528 (Plastics One), which was inserted through the cannula. orexin A (Phoenix Pharmaceuticals) was

529 injected slowly at the dose of 1 nmol dissolved in 2 ul of saline. Starting from 5 days before the injection,
530 mice and the dummy cannula caps were handled for acclimation daily. The locomotion activity was
531 measured in a PhenoMaster System (TSE Systems), and mice were acclimated to the system at least 5
532 days before the test.
533
534 **PET imaging**
535 PET imaging was performed using an Inveon preclinical PET/CT system (Siemens). Male mice were
536 anesthetized with 2% isoflurane in 65%/35% nitrous oxide/oxygen gas, injected with saline or orexin A
537 and positioned on a dedicated mouse carrier (MEDRES, Germany) carrying two mice. Body
538 temperature was maintained at 37.0 ± 0.5°C by a thermostatically controlled water heating system. For
539 injection of the radiotracer, a catheter consisting of a 30G cannula connected to a polythene tubing (ID
540 = 0.28 mm) was inserted into the tail vein and fixated by a drop of glue. After starting the PET scan, 7-
541 8 MBq of [18F]FDG in 50-100 µl saline were injected per mouse. Emission data were acquired for 45
542 minutes. Thereafter, animals were automatically moved into the CT gantry, and a CT scan was
543 performed (180 projections/360°, 200 ms, 80 kV, 500 µA). The CT data were used for attenuation
544 correction of the PET data, and the CT image of the scull was used for image co-registration. Plasma
545 glucose levels were determined from a tail vein blood sample using a standard glucometer (Bayer) after
546 removing the tail vein catheters. PET data were histogrammed in time frames of 12x30s, 3x60s, 3x120s,
547 7x240s, Fourier rebinned, and images were reconstructed using the MAP-SP algorithm provided by the
548 manufacturer. For co-registration, the imaging analysis software Vinci was used (Cizek et al., 2004).
549 Images were co-registered to a 3D mouse brain atlas constructed from the 2D mouse brain atlas
550 published by Paxinos (Paxinos et al., 2013).
551 **Kinetic modeling**
552 An image-derived input function was extracted from the PET data of the aorta, which could be identified
553 in the image of the first time frame of each animal. Input function data were corrected for partial volume
554 effect by assuming a standardized volume fraction of 0.6 (Green et al., 1998). Parametric images of the
555 [18F]FDG kinetic constants K_1, k_2, k_3, and k_4 were determined by a voxel-by-voxel (voxel size = 0.4
556 mm x 0.4 mm x 0.8 mm) fitting of data to a two- tissue-compartment kinetic model. K_1 is the constant

557 for transport from blood to tissue, k_2 for transport from tissue to blood, k_3 the constant for
558 phosphorylation of [18F]FDG to [18F]FDG-6-phosphate, and k_4 the constant for dephosphorylation.
559 The ratio of tissue and plasma glucose concentrations (C_E/C_P) is a measure for glucose transport and is
560 given by $C_E/C_P = K_1/(k_2 + k_3/0.26)$ (Backes et al., 2011; Jais et al., 2016). Since neuronal activation is
561 accompanied by increased glucose transport and this parameter is less sensitive to changes in plasma
562 glucose level, we use alterations of glucose transport (C_E/C_P) as surrogate for alterations in neuronal
563 activation.

564 **Statistics**

565 Statistical testing was performed by application of a voxel-wise t-test between groups. 3D maps of p-
566 values allow for the identification of regions with significant differences in the parameters. From these
567 regions, we defined volumes of interest (VOIs) and performed additional statistical testing for these
568 VOIs. For presentation only, 3D maps of p-values were re-calculated on a 0.1 mm x 0.1 mm x 0.1 mm
569 grid from the original dataset using trilinear interpolation.

570

571 **<u>Virus injection</u>**

572 Male mice received 1 mg/ml of tramadol in drinking water 2 d before the surgeries. On the day of
573 surgery, mice were anesthetized with isoflurane and a bolus of buprenorphine (0.1 mg/kg BW) was
574 given (i. p.) to reduce pain. Brain regions were identified according to the atlas (Franklin & Paxinos,
575 2007). After alignment of the brain in the stereotaxic surgery platform, 1 or 4 small holes were drilled
576 in the skull at specific coordinates. The virus, pAAV-Ef1a-DIO EYFP (~$1x10^{13}$ GC/ml, 300 nl,
577 Addgene) was bilaterally injected into VTA and SN of 10 wk old mice, with micropipettes pulled in
578 house with a heating system. The coordinates from Bregma were: anterior-posterior, AP: -3.4 mm;
579 medial-lateral, ML: ±0.5/1.25 mm; dorsal-ventral, DV: -4.2 mm. The GCaMP6 virus
580 (AAV1.Syn.Flex.GCaMP6s.WPRE.SV40, ~$4x10^{12}$ GC/ml, 300 nl, Penn Vector Core) was injected to
581 left SN (AP: -3.4 mm, ML: 1.1 mm, DV: -4.2 mm) of 12 wk old mice, to specifically express GCaMP6
582 in dopaminergic neurons. After virus injection, mice received a bolus of meloxicam (5 mg/kg BW, s.c.),
583 and tramadol in drinking water for 3 d after surgeries to relieve pain. BW was checked twice a day.
584 Experiments started at least 4 weeks later than virus injection to allow virus expression.

585 **Statistical methods**

586 All values are expressed as the mean ± SEM. Statistical analyses were conducted using
587 GraphPad PRISM (version 8) unless stated otherwise. Datasets with only two independent groups were
588 analyzed for statistical significance using an unpaired two-tailed Student's t-test. Datasets subjected to
589 two independent factors were analyzed using two-way ANOVA followed by Sidak's post hoc test. All
590 p-values < 0.05 were considered significant (*$p < 0.05$, **$p < 0.01$, and ***$p < 0.001$, ****$p < 0.0001$).

Acknowledgements

We acknowledge Hella Brönneke for outstanding support, Jens Alber, Pia Scholl, Christiane Schäfer, Nadine Spenrath, Ina Stünkel, Kerstin Marohl, Antonia Lorenz and Helmut Wratil for outstanding technical assistance. We received funding by the DFG within the framework of the TRR 134 (A.C.H., P.K.), CRC 1451 (P.K.) and within the Excellence Initiative by German Federal and State Governments (CECAD). This work was funded (in part) by the Helmholtz Alliance ICEMED (Imaging and Curing Environmental Metabolic Diseases) through the Initiative and Networking Fund of the Helmholtz Association. X.X. received funding from CECAD Family Support. G.Y. gratefully acknowledges financial doctoral support from the DFG-233886668/GRK1960.

Author Contributions

X.X. and A.C.H. conceived the project, designed the experiments, and wrote the manuscript with input from the other authors. A.C.H. generated the Ox1R flox mouse line. X.X. performed all the experiments apart from calcium imaging experiments (G.Y. and P.K.) and PET imaging experiments (A.L.C. and H.B.). All authors discussed the data, commented on the manuscript before submission, and agreed with the final submitted manuscript.

Competing Interests

The authors declare no competing interests.

References

Arber, S., & Costa, R. M. (2022). Networking brainstem and basal ganglia circuits for movement. *Nat Rev Neurosci*, *23*(6), 342-360. https://doi.org/10.1038/s41583-022-00581-w

Backes, H., Walberer, M., Endepols, H., Neumaier, B., Graf, R., Wienhard, K., & Mies, G. (2011). Whiskers area as extracerebral reference tissue for quantification of rat brain metabolism using (18)F-FDG PET: application to focal cerebral ischemia. *Journal of Nuclear Medicine*, *52*(8), 1252-1260. https://doi.org/10.2967/jnumed.110.085266

Baimel, C., Lau, B. K., Qiao, M., & Borgland, S. L. (2017). Projection-target-defined effects of orexin and dynorphin on VTA dopamine neurons. *Cell Rep*, *18*(6), 1346-1355. https://doi.org/10.1016/j.celrep.2017.01.030

Baykal, S., Albayrak, Y., Durankus, F., Guzel, S., Abbak, O., Potas, N., Beyazyuz, M., Karabekiroglu, K., & Donma, M. M. (2019). Decreased serum orexin A levels in drug-naive children with attention deficit and hyperactivity disorder. *Neurol Sci*, *40*(3), 593-602. https://doi.org/10.1007/s10072-018-3692-8

Berke, J. D. (2018). What does dopamine mean? *Nat Neurosci*, *21*(6), 787-793. https://doi.org/10.1038/s41593-018-0152-y

Berridge, C. W., Espana, R. A., & Vittoz, N. M. (2010). Hypocretin/orexin in arousal and stress. *Brain Res*, *1314*, 91-102. https://doi.org/10.1016/j.brainres.2009.09.019

Capelli, P., Pivetta, C., Soledad Esposito, M., & Arber, S. (2017). Locomotor speed control circuits in the caudal brainstem. *Nature*, *551*(7680), 373-377. https://doi.org/10.1038/nature24064

Cizek, J., Herholz, K., Vollmar, S., Schrader, R., Klein, J., & Heiss, W. D. (2004). Fast and robust registration of PET and MR images of human brain. *Neuroimage*, *22*(1), 434-442. https://doi.org/10.1016/j.neuroimage.2004.01.016

De Bundel, D., Zussy, C., Espallergues, J., Gerfen, C. R., Girault, J. A., & Valjent, E. (2016). Dopamine D2 receptors gate generalization of conditioned threat responses through mTORC1 signaling in the extended amygdala. *Molecular Psychiatry*, *21*(11), 1545-1553. https://doi.org/10.1038/mp.2015.210

de Lecea, L., Kilduff, T. S., Peyron, C., Gao, X., Foye, P. E., Danielson, P. E., Fukuhara, C., Battenberg, E. L., Gautvik, V. T., Bartlett, F. S., 2nd, Frankel, W. N., van den Pol, A. N., Bloom, F. E., Gautvik, K. M., & Sutcliffe, J. G. (1998). The hypocretins: hypothalamus-specific peptides with neuroexcitatory activity. *Proc Natl Acad Sci U S A*, *95*(1), 322-327. https://doi.org/10.1073/pnas.95.1.322

Durairaja, A., & Fendt, M. (2020). Orexin deficiency modulates cognitive flexibility in a sex-dependent manner. *Genes Brain Behav*, e12707. https://doi.org/10.1111/gbb.12707

Eiler, W. J., 2nd, Seyoum, R., Foster, K. L., Mailey, C., & June, H. L. (2003). D1 dopamine receptor regulates alcohol-motivated behaviors in the bed nucleus of the stria terminalis in alcohol-preferring (P) rats. *Synapse*, *48*(1), 45-56. https://doi.org/10.1002/syn.10181

Ekstrand, M. I., Terzioglu, M., Galter, D., Zhu, S., Hofstetter, C., Lindqvist, E., Thams, S., Bergstrand, A., Hansson, F. S., Trifunovic, A., Hoffer, B., Cullheim, S., Mohammed, A. H., Olson, L., & Larsson, N. G. (2007). Progressive parkinsonism in mice with respiratory-chain-deficient dopamine neurons. *Proc Natl Acad Sci U S A*, *104*(4), 1325-1330. https://doi.org/10.1073/pnas.0605208103

Fadel, J., & Deutch, A. Y. (2002). Anatomical substrates of orexin–dopamine interactions: lateral hypothalamic projections to the ventral tegmental area. *Neuroscience*, *111*(2), 379-387. https://doi.org/https://doi.org/10.1016/S0306-4522(02)00017-9

Feldman, H. M., & Reiff, M. I. (2014). Clinical practice. Attention deficit-hyperactivity disorder in children and adolescents. *N Engl J Med*, *370*(9), 838-846. https://doi.org/10.1056/NEJMcp1307215

Franklin, K. B. J., & Paxinos, G. (2007). *The mouse brain in stereotaxic coordinates* (3rd ed.). Elsevier/Academic Press.

Freeman, L. R., Bentzley, B. S., James, M. H., & Aston-Jones, G. (2021). Sex differences in demand for highly palatable foods: role of the orexin system. *Int J Neuropsychopharmacol*, *24*(1), 54-63. https://doi.org/10.1093/ijnp/pyaa040

Furlong, T. M., Vianna, D. M., Liu, L., & Carrive, P. (2009). Hypocretin/orexin contributes to the expression of some but not all forms of stress and arousal. *Eur J Neurosci*, *30*(8), 1603-1614. https://doi.org/10.1111/j.1460-9568.2009.06952.x

Giardino, W. J., Eban-Rothschild, A., Christoffel, D. J., Li, S. B., Malenka, R. C., & de Lecea, L. (2018). Parallel circuits from the bed nuclei of stria terminalis to the lateral hypothalamus drive opposing emotional states. *Nat Neurosci*, *21*(8), 1084-1095. https://doi.org/10.1038/s41593-018-0198-x

Gonzalez, J. A., Iordanidou, P., Strom, M., Adamantidis, A., & Burdakov, D. (2016). Awake dynamics and brain-wide direct inputs of hypothalamic MCH and orexin networks. *Nat Commun*, *7*, 11395. https://doi.org/10.1038/ncomms11395
Green, L. A., Gambhir, S. S., Srinivasan, A., Banerjee, P. K., Hoh, C. K., Cherry, S. R., Sharfstein, S., Barrio, J. R., Herschman, H. R., & Phelps, M. E. (1998). Noninvasive methods for quantitating blood time-activity curves from mouse PET images obtained with fluorine-18-fluorodeoxyglucose. *Journal of Nuclear Medicine*, *39*(4), 729-734. <Go to ISI>://WOS:000072956600042
Howe, M. W., & Dombeck, D. A. (2016). Rapid signalling in distinct dopaminergic axons during locomotion and reward. *Nature*, *535*(7613), 505-510. https://doi.org/10.1038/nature18942
Hrabovszky, E., Molnar, C. S., Borsay, B. A., Gergely, P., Herczeg, L., & Liposits, Z. (2013). Orexinergic input to dopaminergic neurons of the human ventral tegmental area. *PLoS One*, *8*(12), e83029. https://doi.org/10.1371/journal.pone.0083029
Inutsuka, A., & Yamanaka, A. (2013). The physiological role of orexin/hypocretin neurons in the regulation of sleep/wakefulness and neuroendocrine functions. *Front Endocrinol (Lausanne)*, *4*, 18. https://doi.org/10.3389/fendo.2013.00018
Jais, A., Solas, M., Backes, H., Chaurasia, B., Kleinridders, A., Theurich, S., Mauer, J., Steculorum, S. M., Hampel, B., Goldau, J., Alber, J., Förster, C. Y., Eming, S. A., Schwaninger, M., Ferrara, N., Karsenty, G., & Brüning, J. C. (2016). Myeloid-cell-derived VEGF maintains brain glucose uptake and limits cognitive impairment in obesity. *Cell*, *165*(4), 882-895. https://doi.org/10.1016/j.cell.2016.03.033
Jordan, S. D., Kruger, M., Willmes, D. M., Redemann, N., Wunderlich, F. T., Bronneke, H. S., Merkwirth, C., Kashkar, H., Olkkonen, V. M., Bottger, T., Braun, T., Seibler, J., & Bruning, J. C. (2011). Obesity-induced overexpression of miRNA-143 inhibits insulin-stimulated AKT activation and impairs glucose metabolism [Research Support, Non-U.S. Gov't]. *Nat Cell Biol*, *13*(4), 434-446. https://doi.org/10.1038/ncb2211
Kitahama, K., Nagatsu, I., Geffard, M., & Maeda, T. (2000). Distribution of dopamine-immunoreactive fibers in the rat brainstem. *Journal of Chemical Neuroanatomy*, *18*(1-2), 1-9. https://doi.org/Doi 10.1016/S0891-0618(99)00047-2
Koblinger, K., Jean-Xavier, C., Sharma, S., Fuzesi, T., Young, L., Eaton, S. E. A., Kwok, C. H. T., Bains, J. S., & Whelan, P. J. (2018). Optogenetic activation of A11 region increases motor activity. *Front Neural Circuits*, *12*, 86. https://doi.org/10.3389/fncir.2018.00086
Korotkova, T. M., Eriksson, K. S., Haas, H. L., & Brown, R. E. (2002). Selective excitation of GABAergic neurons in the substantia nigra of the rat by orexin/hypocretin in vitro. *Regul Pept*, *104*(1-3), 83-89. https://doi.org/10.1016/s0167-0115(01)00323-8
Korotkova, T. M., Sergeeva, O. A., Eriksson, K. S., Haas, H. L., & Brown, R. E. (2003). Excitation of ventral tegmental area dopaminergic and nondopaminergic neurons by orexins/hypocretins. *J Neurosci*, *23*(1), 7-11. https://www.ncbi.nlm.nih.gov/pubmed/12514194
Krawczyk, M., Mason, X., DeBacker, J., Sharma, R., Normandeau, C. P., Hawken, E. R., Di Prospero, C., Chiang, C., Martinez, A., Jones, A. A., Doudnikoff, E., Caille, S., Bezard, E., Georges, F., & Dumont, E. C. (2013). D1 dopamine receptor-mediated LTP at GABA synapses encodes motivation to self-administer cocaine in rats. *Journal of Neuroscience*, *33*(29), 11960-+. https://doi.org/10.1523/Jneurosci.1784-13.2013
Lebestky, T., Chang, J. S., Dankert, H., Zelnik, L., Kim, Y. C., Han, K. A., Wolf, F. W., Perona, P., & Anderson, D. J. (2009). Two different forms of arousal in Drosophila are oppositely regulated by the dopamine D1 receptor ortholog DopR via distinct neural circuits. *Neuron*, *64*(4), 522-536. https://doi.org/10.1016/j.neuron.2009.09.031
Lima, S. Q., & Miesenbock, G. (2005). Remote control of behavior through genetically targeted photostimulation of neurons. *Cell*, *121*(1), 141-152. https://doi.org/10.1016/j.cell.2005.02.004
Lippert, R. N., Hess, S., Klemm, P., Burgeno, L. M., Jahans-Price, T., Walton, M. E., Kloppenburg, P., & Bruning, J. C. (2020). Maternal high-fat diet during lactation reprograms the dopaminergic circuitry in mice. *J Clin Invest*, *130*(7), 3761-3776. https://doi.org/10.1172/JCI134412
Liu, C., Xue, Y., Liu, M. F., Wang, Y., Liu, Z. R., Diao, H. L., & Chen, L. (2018). Orexins increase the firing activity of nigral dopaminergic neurons and participate in motor control in rats. *J Neurochem*, *147*(3), 380-394. https://doi.org/10.1111/jnc.14568
Mahler, S. V., Moorman, D. E., Smith, R. J., James, M. H., & Aston-Jones, G. (2014). Motivational activation: a unifying hypothesis of orexin/hypocretin function. *Nat Neurosci*, *17*(10), 1298-1303. https://doi.org/10.1038/nn.3810

Mahler, S. V., Smith, R. J., Moorman, D. E., Sartor, G. C., & Aston-Jones, G. (2012). Multiple roles for orexin/hypocretin in addiction. *Prog Brain Res*, *198*, 79-121. https://doi.org/10.1016/B978-0-444-59489-1.00007-0
Marcus, J. N., Aschkenasi, C. J., Lee, C. E., Chemelli, R. M., Saper, C. B., Yanagisawa, M., & Elmquist, J. K. (2001). Differential expression of orexin receptors 1 and 2 in the rat brain. *J Comp Neurol*, *435*(1), 6-25. https://doi.org/10.1002/cne.1190
Nair-Roberts, R. G., Chatelain-Badie, S. D., Benson, E., White-Cooper, H., Bolam, J. P., & Ungless, M. A. (2008). Stereological estimates of dopaminergic, GABAergic and glutamatergic neurons in the ventral tegmental area, substantia nigra and retrorubral field in the rat. *Neuroscience*, *152*(4), 1024-1031. https://doi.org/10.1016/j.neuroscience.2008.01.046
Nakamura, T., Uramura, K., Nambu, T., Yada, T., Goto, K., Yanagisawa, M., & Sakurai, T. (2000). Orexin-induced hyperlocomotion and stereotypy are mediated by the dopaminergic system. *Brain Res*, *873*(1), 181-187. https://doi.org/10.1016/s0006-8993(00)02555-5
Narayanan, N. S., Guarnieri, D. J., & DiLeone, R. J. (2010). Metabolic hormones, dopamine circuits, and feeding. *Front Neuroendocrinol*, *31*(1), 104-112. https://doi.org/10.1016/j.yfrne.2009.10.004
Palmiter, R. D. (2007). Is dopamine a physiologically relevant mediator of feeding behavior? *Trends in Neurosciences*, *30*(8), 375-381. https://doi.org/10.1016/j.tins.2007.06.004
Paxinos, G., Franklin, K. B. J., & Franklin, K. B. J. (2013). *Paxinos and Franklin's the mouse brain in stereotaxic coordinates* (4th ed.). Elsevier/Academic Press.
Peyron, C., Tighe, D. K., van den Pol, A. N., de Lecea, L., Heller, H. C., Sutcliffe, J. G., & Kilduff, T. S. (1998). Neurons containing hypocretin (orexin) project to multiple neuronal systems. *J Neurosci*, *18*(23), 9996-10015. https://doi.org/10.1523/JNEUROSCI.18-23-09996.1998
Roeper, J. (2013). Dissecting the diversity of midbrain dopamine neurons. *Trends in Neurosciences*, *36*(6), 336-342. https://doi.org/https://doi.org/10.1016/j.tins.2013.03.003
Ruud, J., Alber, J., Tokarska, A., Engstrom Ruud, L., Nolte, H., Biglari, N., Lippert, R., Lautenschlager, A., Cieslak, P. E., Szumiec, L., Hess, M. E., Bronneke, H. S., Kruger, M., Nissbrandt, H., Korotkova, T., Silberberg, G., Rodriguez Parkitna, J., & Bruning, J. C. (2019). The fat mass and obesity-associated protein (FTO) regulates locomotor responses to novelty via D2R medium spiny neurons. *Cell Rep*, *27*(11), 3182-3198 e3189. https://doi.org/10.1016/j.celrep.2019.05.037
Sakurai, T., Amemiya, A., Ishii, M., Matsuzaki, I., Chemelli, R. M., Tanaka, H., Williams, S. C., Richardson, J. A., Kozlowski, G. P., Wilson, S., Arch, J. R. S., Buckingham, R. E., Haynes, A. C., Carr, S. A., Annan, R. S., McNulty, D. E., Liu, W.-S., Terrett, J. A., Elshourbagy, N. A., . . . Yanagisawa, M. (1998). Orexins and orexin receptors: a family of hypothalamic neuropeptides and G protein-coupled receptors that regulate feeding behavior. *Cell*, *92*(4), 573-585. https://doi.org/https://doi.org/10.1016/S0092-8674(00)80949-6
Sharples, S. A., Koblinger, K., Humphreys, J. M., & Whelan, P. J. (2014). Dopamine: a parallel pathway for the modulation of spinal locomotor networks. *Front Neural Circuits*, *8*, 55. https://doi.org/10.3389/fncir.2014.00055
Soya, S., & Sakurai, T. (2020). Evolution of orexin neuropeptide system: structure and function. *Front Neurosci*, *14*, 691. https://doi.org/10.3389/fnins.2020.00691
Takatoh, J., Nelson, A., Zhou, X., Bolton, M. M., Ehlers, M. D., Arenkiel, B. R., Mooney, R., & Wang, F. (2013). New modules are added to vibrissal premotor circuitry with the emergence of exploratory whisking. *Neuron*, *77*(2), 346-360. https://doi.org/10.1016/j.neuron.2012.11.010
Tsujino, N., & Sakurai, T. (2013). Role of orexin in modulating arousal, feeding, and motivation. *Front Behav Neurosci*, *7*, 28. https://doi.org/10.3389/fnbeh.2013.00028
Tung, L. W., Lu, G. L., Lee, Y. H., Yu, L., Lee, H. J., Leishman, E., Bradshaw, H., Hwang, L. L., Hung, M. S., Mackie, K., Zimmer, A., & Chiou, L. C. (2016). Orexins contribute to restraint stress-induced cocaine relapse by endocannabinoid-mediated disinhibition of dopaminergic neurons. *Nat Commun*, *7*, 12199. https://doi.org/10.1038/ncomms12199
Turiault, M., Parnaudeau, S., Milet, A., Parlato, R., Rouzeau, J. D., Lazar, M., & Tronche, F. (2007). Analysis of dopamine transporter gene expression pattern -- generation of DAT-iCre transgenic mice. *FEBS J*, *274*(14), 3568-3577. https://doi.org/10.1111/j.1742-4658.2007.05886.x
Volkow, N. D., & Swanson, J. M. (2013). Clinical practice: Adult attention deficit-hyperactivity disorder. *N Engl J Med*, *369*(20), 1935-1944. https://doi.org/10.1056/NEJMcp1212625
Xiao, X., Yeghiazaryan, G., Hess, S., Klemm, P., Sieben, A., Kleinridders, A., Morgan, D. A., Wunderlich, F. T., Rahmouni, K., Kong, D., Scammell, T. E., Lowell, B. B., Kloppenburg, P., Brüning,

J. C., & Hausen, A. C. (2021). Orexin receptors 1 and 2 in serotonergic neurons differentially regulate peripheral glucose metabolism in obesity. *Nature Communications*, *12*(1), 5249. https://doi.org/10.1038/s41467-021-25380-2